Journal of Alloys and Compounds 581 (2013) 646–652

Contents lists available at ScienceDirect

Journal of Alloys and Compounds

journal homepage: www.elsevier.com/locate/jalcom

Hot-injection synthesis and characterization of monodispersed ternary Cu_2SnSe_3 nanocrystals for thermoelectric applications

Ji-Ming Song *, Yu Liu, He-Lin Niu, Chang-Jie Mao, Long-Jiu Cheng, Sheng-Yi Zhang, Yu-Hua Shen

School of Chemistry and Chemical Engineering, Key Laboratory of Functional Inorganic Materials Chemistry of Anhui Province, Anhui University, Hefei, Anhui 230039, PR China

ARTICLE INFO

Article history:
Received 12 April 2013
Received in revised form 15 July 2013
Accepted 18 July 2013
Available online 1 August 2013

Keywords:
Cu_2SnSe_3
Nanocrystals
Schlenk line technique
Hot-injection
Thermoelectric properties

ABSTRACT

Cu_2SnSe_3 (copper tin selenide, CTSe) is one of promising copper-based selenides materials in the use of acousto-optic and photovoltaic fields. In this communication, the CTSe nanocrystals was successfully synthesized by a "hot-injection" protocol in the presence of oleylamine (OLA). Selenium powder dissolved in the mixed solution of OLA and dodecanethiol (DT) were injected into a hot solution of OLA, including copper chloride, tin chloride, at a given reaction temperature. The structure, composition and morphology of the synthesized samples were characterized via using powder X-ray diffraction (XRD), X-ray photoelectron spectroscopy (XPS), transmission electron microscopy (TEM) and field-emission scanning electron microscopy (SEM). The results revealed that the as-synthesized nanocrystals were single phase polycrystalline, cubic crystal structure, and high monodispersity with an average diameter of 5 nm. The thermoelectric properties of these dense materials compacted from nanocrystals with the temperature range from 300 K to 598 K were studied. The results exhibit a promising figure-of-merit *ZT* at 598 K, and it demonstrates that the prepared CTSe could potentially be useful for efficient thermoelectric materials.

1. Introduction

Thermoelectric (TE) materials have attracted much attention for their potential applications in power generation, cooling, and thermal sensing. Seeking inexpensive materials with high TE performance has been a focus for materials science for decades, and it may arouse a revolution in energy saving and environmental protection if possible and this task becomes even more urgently needed in recent years [1,2]. Ideal TE materials possess low thermal conductivity with good electrical conductivity. Compacting wet-chemistry-synthesized nanoparticles into dense samples is expected to be an efficient strategy to achieve low thermal conductivity due to the enhanced scattering of phonons at the numerous grain boundaries [3]. The dimensionless TE figure of merit, defined as ZT ($ZT = \sigma S^2 T/\kappa$), where σ, S, T, and κ are the electric conductivity, the Seebeck coefficient, the absolute temperature, and the thermal conductivity, respectively. The correlation of these parameters results in a very limited choice of the currently state-of-the-art TE materials.

At present, some high-performance TE materials have been developed, including alloys of the forms $(AgSbTe_2)_{100-x}(GeTe)_x$ (TAGS) system and the PbTe-based system. Due to their superior thermoelectric properties and sufficient mechanical robustness, TAGS-85 and a *p*-type PbTe-based material have been successfully used in applications [4,5]. In addition, copper-based multinary semiconductors have recently emerged as some of the best performing *p*-type TE materials. It is reported that copper chalcogenides, such as BiCuSeO based compounds, have high ZT values and an excellent charge transport behavior ($ZT = 0.81$ and 1.1, at 923 K). The ZT value of 1.1 is higher than that of any TE oxide reported so far and is close to the values observed in most of the TE metallic alloys [6,7]. One potentially attractive, yet not well studied, copper-based material is CTSe. The CTSe is one of the most important group I_2–IV–VI_3 family of compound semiconductors that possesses a direct band gap in the range of $Eg = 0.8$–1.1 eV, a high absorption coefficient ($\sim 10^4$–10^5 cm^{-1}) [8–10], and electron and hole mobilities on the order of ~ 2 and ~ 870 $cm^2 V^{-1} s^{-1}$ [8,11], respectively, for bulk material. CTSe has a cubic sphalerite-like phase ($a = 5.69$ Å, space group $F\bar{4}3m$) and a monoclinic phase with a sphalerite superstructure ($a = 6.59$, $b = 12.16$, and $c = 6.61$ Å; $\beta = 108.6°$; space group Cc) [12]. It is similar to other copper-based ternary or more polynary nanoparticles – such as $CuInSe_2$ [13], $CuFeS_{2-x}/S_2$ [14,15], $CuGaTe_2$ [16], Cu_3SbSe_4–Cu_3SbS_4 [17], $Cu_2ZnSnS_4/Se_4/Te_4$ [18], $Cu_2CdSnSe_4$ [19–21], $Cu_{1-x}Pt_xFeO_2$ [22], and $Cu_2ZnSn_{1-x}In_xSe_4$ [23]. CTSe also shows promising TE semiconductor with a relatively high electrical conductivity and moderate thermal conductivity, and it may be widely used in industry for small-scale cooling components and low-temperature power generators. Recently, the phase-pure CTSe has been prepared only a few examples, as bulk by vertical Bridgman–Stockbarger technique [24,25], as thin films by co-evaporation

* Corresponding author. Tel./fax: +86 0551 65107342.
E-mail address: jiming@ahu.edu.cn (J.-M. Song).

0925-8388/$ - see front matter © 2013 Elsevier B.V. All rights reserved.
http://dx.doi.org/10.1016/j.jallcom.2013.07.119

technique [8], and as nanocrystals by colloidal synthesis [26–28]. However, they require either complex and hazardous precursors or long reaction time. As we have seen, the conventional colloidal synthesis of ternary or polynary selenides nanocrystals usually involves the preparation of soluble Se precursors using alkylphosphines, such as trioctylphosphine (TOP) [27,29], and tributylphosphine (TBP) [30]. Elemental Se can be easily dissolved in TOP, but TOP itself is very sensitive to oxygen and need to be handled in a glovebox, which is not favorable for a large-scale synthesis. It is, therefore, essential to find a facile way to synthesis of high-quality selenide nanocrystals from low cost chemicals. Recently, the colloidal synthesis of monodispersed ternary and more polynary copper-based nanocrystals has been a hot issue due to their potential applications as inorganic solar absorbers in photovoltaics and photodetector devices [26,28,31]. However, colloidal synthesis of monodispersed CTSe nanocrystals and the study of the TE properties of dense materials compacted from CTSe nanocrystals are still rare.

Herein, we report on the successful synthesis of crystalline ternary CTSe nanocrystals in large-scale, high-quality, via solution-phase approach in Schlenk line under N_2 flow. In the present study, low-toxicity, inexpensive Se precursor, which was obtained from Se powder dissolution in OLA and DT at room temperature, was used. This Se precursor was highly reactive and suitable for the synthesis of CTSe nanocrystals. The as-prepared CTSe nanocrystals possess high size uniform, monodispersity and disperse readily in various nonpolar solvents. In addition, the results from the characterization of the electrical and TE properties of the CTSe nanocrystals are also presented here, and a high peak *ZT* value can be obtained at the temperature of 598 K.

2. Experimental

2.1. Chemicals

Copper (II) chloride dehydrate ($CuCl_2{\cdot}2H_2O$, 99%), tin (II) chloride dihydrate ($SnCl_2{\cdot}2H_2O$, 98%), selenium powder (99.5%), dodecanethiol (DT, 98%) and oleylamine (OLA, 80–90%) were purchased from Aladdin. All of analytical grade including, hexane (97%), $N_2H_4{\cdot}H_2O$ (85%), ethanol and chloroform were purchased from Sinopharm Chemical Reagent Co., Ltd. They were used in experiments without further purification.

All synthesis was carried out by using standard airless techniques: a vacuum/dry nitrogen gas Schlenk line was used for the synthesis and handling air and moisture-sensitive chemicals.

2.2. Synthesis of Cu_2SnSe_3 nanocrystals

A typical experimental procedure was as follows:

(1) **Preparation of stocksolution**:**(a) stocksolution**, 3.0 ml OLA, 3.0 ml DT and 3.0 mmol Se powder were loaded into a 100 ml three-neck flask at room temperature, cycled between vacuum and nitrogen three times to remove the oxygen in the flask, and then stirred under a nitrogen atmosphere for dissolving Se powder to get (a) stock solution. **(b) stocksolution**, In the meanwhile, 2.0 mmol $CuCl_2{\cdot}2H_2O$, 1.0 mmol $SnCl_2{\cdot}H_2O$, 10 ml OLA and 1 ml DT were mixed in another three-neck flask at room temperature, and cycled between vacuum and nitrogen three times too. Afterward, the solution was kept at 60 °C under vacuum for 30 min, and then heated to 180 °C to obtain the (b) stock solution. During the reaction, the color of the solution changed from blue to milky at 60 °C, and finally to brown at the temperature of over 150 °C.

(2) **The synthesis of CTSenanocrystals**: After the Se powder was completely dissolved, the 6 ml of (a) stock solution was quickly injected into the reaction vessel of (b) stock solution under magnetic stirring and the color of the solution changed immediately from light brown to dark brown, indicating that the nucleation and subsequent growth of CTSe nanostructures occurred. After injection, the temperature of the reaction mixture dropped to ~170 °C, and it was allowed to recover to the pre-injection temperature (180 °C). The overall reaction time after recover to 180 °C was 30 min, and then the sample was rapidly cooled to room temperature to achieve CTSe nanocrystals. The brown-black product was centrifuged at 8000 rpm for 10 min and collected. The upper yellow solution was discarded and the obtained products were washed with chloroform and ethanol. For XRD, SEM, TEM and hot-pressing, the washing procedure needed to be repeated at least 5 cycles until the products could not be dispersed in hexane any more. The product was then dried in the oven for 3 h and collected for characterization.

2.3. Characterization of samples

The phase purity and the crystallinity of the sample were characterized by powder X-ray diffraction and the 2θ angle varied from 10° to 80° at a scanning rate of 4°/min (XRD, Rigaku D/max-RA, graphite monochromatized Cu Kα radiation, λ = 0.15406 Å). X-ray photoelectron spectroscopy (XPS) was performed by using a VG ESCA scientific theta probe spectrometer in constant analyzer energy mode with a pass energy of 28 eV and Al Ka (1486.6 eV) radiation as the excitation source. Transmission electron microscopy (TEM) and high resolution TEM (HRTEM) observation were performed on Hitachi JEM-2100 instruments with an acceleration voltage of 200 kV. The morphologies of the nanocrystals after removing the capping ligands, and the fracture of the hot-pressed pellets were characterized using field-emission scanning electron microscopy (SEM, S4800, Hitachi, Japan, at 5.0 kV). Inductively coupled plasma atomic emission spectrometry (ICP-AES) measurements were conducted using Vario ELIII (Elementar Analysensyteme Gmbh, Germany).

2.4. TE property measurements

The possibly residual organic surfactants were removed via the following methods before fabrication of bulk samples for TE measurement. To remove any organic ligands, the nanocrystals were stirred in a mixture of 85% hydrazine (CAUTION: please note that hydrazine should be handled with extreme caution due to its high toxicity) and hexane with volume ratio of 1:2 for 4–6 h until the nanocrystals effortlessly went into to the hydrazine phase and the hexane phase appeared completely transparent. Then the upper hexane phase was removed and fresh hexane was added. This process was repeated for 3 cycles. Finally, the hydrazine-capped nanocrystals were collected by centrifugation and vacuum-dried for hot-pressing. The obtained powder (about 1.6 g) was loaded into a graphite die and compacted into a dense material under a uniaxial pressure of 48 MPa at 623 K for 20 min in an Ar atmosphere for TE transport measurement. For electrical conductivity and Seebeck coefficient measurements, the sample for about 1.5 mm × 1.5 mm × 10 mm was measured by a commercial four-probe apparatus (ULVAC–RIKO ZEM-3). Thermal diffusivity λ was obtained by laser flash method (Netzsch LFA457) performed on round disc samples with a diameter of about 12.5 mm, thickness of 2.5 mm and a diameter of 20 mm, thickness less than 1 mm for parallel and perpendicular measurement, respectively. Specific heat *Cp* was measured on DSC–Q2000 (TA) using Sapphire as calibration sample. The thermal conductivity was calculated from $\kappa = \lambda C_p \rho$, where ρ is the density of the sample determined by Archimedes' method. All the electrical and thermal transport properties have been measured along the perpendicular and parallel to the hot press direction to evaluate the anisotropic properties of CTSe.

3. Results and discussion

CTSe nanocrystals were synthesized by a "hot-injection" protocol in which we injected selenium precursor into a hot solution at a given reaction temperature. It is reported that Se powder cannot be dissolved in DT or OLA alone but can dissolve in their mixture, in which Se powder is reduced by DT, whereas DT is oxidized to disulfides ($m\mathrm{OLA} + n\mathrm{Se} + \mathrm{HS}-\mathrm{C_{12}H_{25}} \rightarrow (\mathrm{OLA})_m\mathrm{Se}_n + \mathrm{H_{25}C_{12}}-\mathrm{S}-\mathrm{S}-\mathrm{C_{12}H_{25}}$) [31]. Fig. 1a shows an X-ray diffraction (XRD) pattern of the products obtained by this colloidal synthesis approach. A clean set of peaks indicate high purity of the sample. The intensity and the position of the peaks suggest that the products indexed to cubic CTSe (space group of $F\bar{4}3m$), which is in good agreement with the reported data (Joint Committee on Powder Diffraction Standards, JCPDS card No. 89-2879). No diffraction signal from impurities is present in the pattern. The results show that the sample prepared had main diffraction peaks at 2θ of 27.1°, 45.0°, and 53.4°, representing the corresponding indices of (111), (220), and (311) orientations of the CTSe nanocrystals, respectively. The chemical composition of the CTSe nanocrystals obtained was very close to the stoichiometry ratio of 2:1:3 (Cu/Sn/Se) as determined from ICP analysis (2.03:1:2.98). Fig. 1b shows the cubic cell composed of CTSe tetrahedrons (unit cell parameter a = 0.569 nm) with Cu and Sn atoms randomly occupying the same positions of the surface and edges in an occupancy ratio corresponding to $Cu_{2/3}/Sn_{1/3}$.

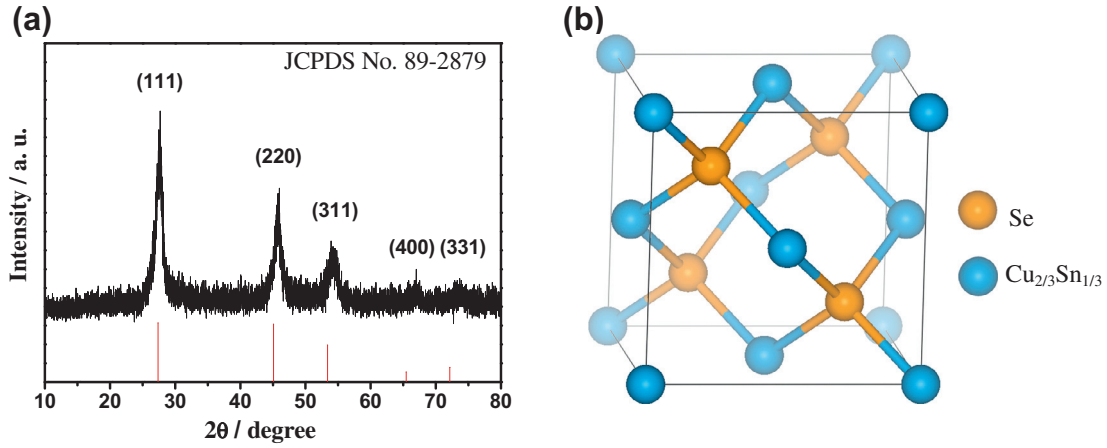

Fig. 1. (a) XRD pattern for the sample of CTSe and the red vertical is the standard literature data. (b) Unit cell of cubic CTSe. (For interpretation of the references to color in this figure legend, the reader is referred to the web version of this article.)

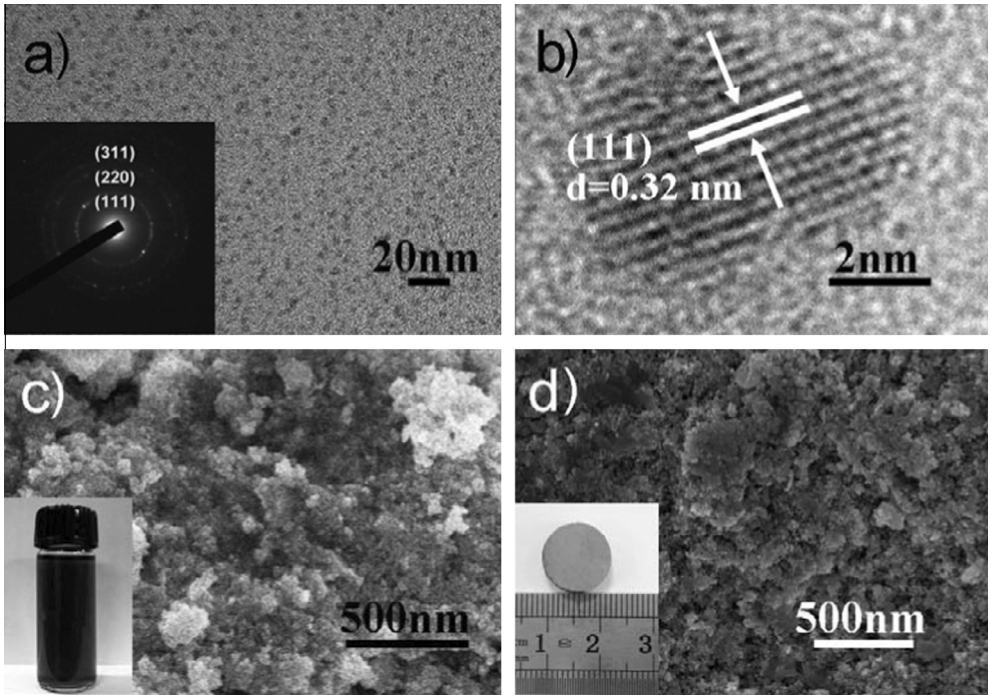

Fig. 2. (a) A general overview TEM image of CTSe nanocrystals. The inset in (a) shows selective-area electron diffraction (SAED). (b) HRTEM image of single CTSe nanocrystals, showing that it is well crystallized. (c) SEM image shows the surface-clean CTSe nanocrystals. The inset in (c) shows that a photograph of a vial of solution containing stably suspended CTSe nanocrystals. (d) SEM image of the fracture surface of bulk material compacted from CTSe nanocrystals after the hot-pressing temperature of 623 K. The inset in (d) shows photograph of the hot-pressed pellet.

The size distribution and morphology of the synthesized nanocrystals are characterized by TEM. The CTSe nanocrystals are nearly monodisperse nanoparticles with an average diameter of 5 nm (Fig. 2a). The obtained nanocrystals can be well dispersed in non-polar solvents, such as hexane, toluene, and chloroform, to form stable, dark-brown dispersions. The CTSe nanocrystals are dispersed in chloroform as shown in the inset of Fig. 2c. This dark-brown solution was stable and no noticeable precipitation was noted during the period of our observation (>3 months). The HRTEM image obtained on a typical CTSe single nanocrystal indicates that it is well crystallized, and the lattice space of d = 0.32 nm, consistent with the (1 1 1) crystallographic facet of ternary CTSe (Fig. 2b). The SEM images of the surface-clean nanocrystals and the fracture surfaces of hot-pressed cylinder are presented in Fig. 2c and d, respectively, and the inset in (d) shows photograph of the hot-pressed pellet.

XPS was performed to investigate the chemical electronic state of the as-prepared CTSe nanocrystals as shown in Fig. 3a. High-resolution spectra of Cu 2p, Sn 3d, and Se 3d were measured to determine the oxidation states of the constituent elements. The narrow doublet peaks in the Cu 2p spectrum appear at 931.7 eV ($2p_{3/2}$) and 951.5 eV ($2p_{1/2}$), which is consistent with the standard separation of 19.8 eV and indicative of Cu (I) [32,33] (Fig. 3b). In addition, the Cu $2p_{3/2}$ satellite peak of Cu (II), which is usually located at 942 eV ($2p_{3/2}$) [34], does not appear in the spectrum. Therefore, it can be concluded that only monovalent copper exists in the sample. The peaks of Sn 3d appear at binding energies of 487.15 eV ($3d_{5/2}$) and 495.55 eV ($3d_{3/2}$), which can be assigned to Sn (IV) with

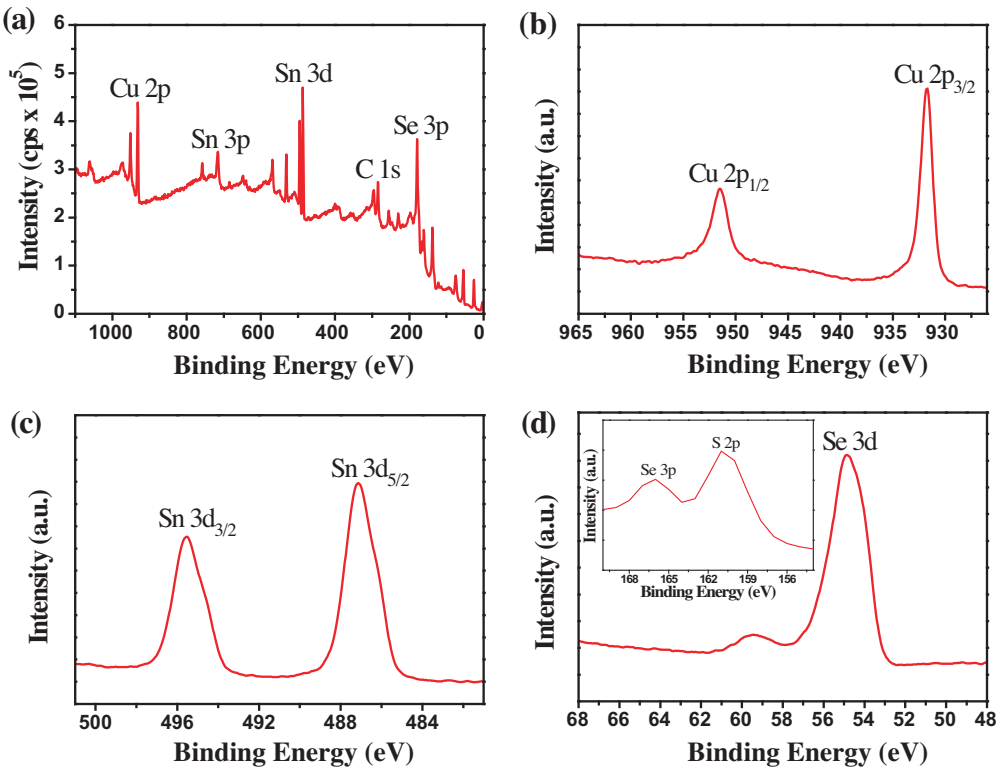

Fig. 3. The XPS spectrum of the obtained CTSe nanocrystals: (a) CTSe, (b) Cu 2p, (c) Sn 3d, and (d) Se 3d and the inset shows the spectrum of Se 3p and S 2p.

a peak splitting of 8.4 eV [33,35] (Fig. 3c). Fig. 3d shows the Se $3d_{5/2}$ peak located at 54.75 eV, indicating Se with a valence of −2. From the inset of Fig. 3d, the Se 3p core located at 166.7 eV, which are in good accordance with values reported previously, being assigned to Se $3p_{1/2}$ [32,36]. The peak which located at 161.7 eV in the inset spectra of Fig. 3d was assigned to S 2p [33].

To characterize the TE properties of compacted bulk materials made from CTSe nanocrystals, 1.6 g of surface-clean products were hot-pressed into dense pellet under the uniaxial pressure of 48 MPa at 623 K (with the rising temperature 5 K/min) for 20 min. The density of the pellet is 3.8 g/cm^3 according to the Archimedes' method, which is approximately 90.5% of the relative theory value. It can be seen from the inset photograph in Fig. 2d that the dense pellet hot-pressed at 623 K have an obvious metallic luster, and the pellet is mechanically robust enough to endure the dicing and polishing process. It can observe that the coalescence and re-growth of nanocrystals are obvious after hot-pressing at the temperature of 623 K from the TEM as shown in Fig. 4a. The TEM image also indicates that the large grains with diameters of several hundred nanometers observed by SEM (Fig. 2d) are actually composed of smaller features. The re-growth and coalescence of the CTSe nanocrystals can be further confirmed through the X-ray diffraction (XRD) analysis, where we find the full-width-half-maxima (FWHM) of the diffraction peaks are much narrower than that of the original XRD of CTSe nanocrystals (Fig. 4b). The high processing temperatures resulted in the formation of CuSe as a secondary phase. The XRD of the product shows that the re-growth sample had several weak diffraction peaks of CuSe on the basis of the original XRD of the CTSe. The size of some of the coalesced nanocrystals further increases to around 16 nm, which calculated from the fitting of the XRD patterns using Scherrer's equation. The composition of CTSe nanocrystals after hot press was 2.03:0.92:2.98 (Cu/Sn/Se) as determined from ICP analysis, from which we can see that these nanocrystals is a slight Sn insufficient.

The TE properties of the CTSe nanocrystals were measured in the temperature range from 300 K to 598 K. Two bar samples with

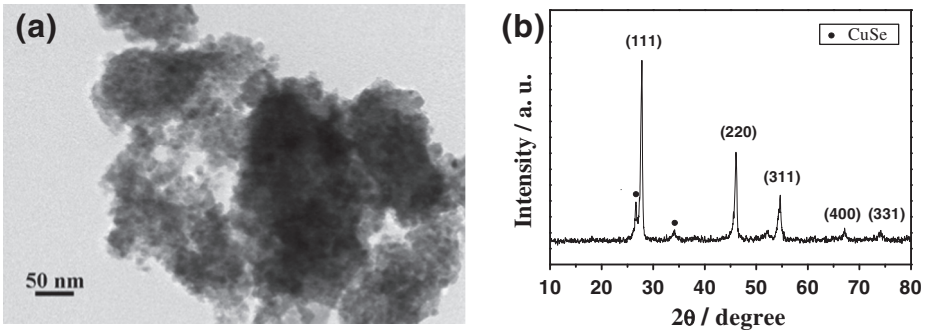

Fig. 4. (a) TEM image shows CTSe nanocrystals after the hot-pressing temperature of 623 K. (b) XRD pattern of hot pressed CTSe cylinder. Some weak diffraction peaks of the sample split due to the re-growth of nanocrystals.

dimensions about 1.5 mm × 1.5 mm × 10 mm were diced from the disk samples for measuring the electric conductivities (σ) and Seebeck coefficients (S) along parallel and perpendicular to the press directions. For the CTSe hot-pressed dense material, the electrical conductivity is largely enhanced [27]. It found that the electric conductivities decrease monotonously with the temperature in both directions as shown in Fig. 5a. The electric conductivities of the sample fall in the ranges of $1.440 \times 10^4\ Sm^{-1}$ to $1.190 \times 10^4\ Sm^{-1}$ (perpendicular) and $1.430 \times 10^4\ Sm^{-1}$ to $1.185 \times 10^4\ Sm^{-1}$ (parallel) from room temperature to 598 K, respectively, which is larger than the previously reported undoped CTSe [27] at the given temperatures. Previous research found that In-doped CTSe bulk materials showed drastic enhancement of σ, and the improvements were attributed to the creation of p-type carriers, which resulted in the improvement of power factor (PF) within the whole temperature range [37]. Herein, besides the Sn vacancies, the minor CuSe in our dense material would further increase the carrier concentration. Fig. 5a also shows that electrical conductivity along the perpendicular direction is a little higher than that of parallel direction, which evidences that a significant anisotropic characteristic. The Seebeck coefficients of all samples are positive, being indicative of a p-type electrical transport property, and the Seebeck coefficients increase with temperature monotonously rising in both directions as shown in Fig. 5b. The Seebeck coefficients of the samples reach the peak value of about 299 μV/K and 299.8 μV/K (Table 1) in the directions of perpendicular and parallel to the press direction at 598 K, respectively, which are a little higher than those of undoped and In-doped CTSe bulk [27,37]. Based on the results of electrical conductivity and the Seebeck coefficient, the PF of the samples can be calculated according to the equation $PF = \sigma S^2$. It notice that the PF increase monotonously with the temperature rising (Fig. 5c), peaking around 1.07 mW m^{-1} K^{-2} (perpendicular) and 1.06 mW m^{-1} K^{-2} (parallel) (Table 1), which are higher than the state-of-the-art value in Ref. [27] at a nearby temperature of 598 K, and the value itself is much close to the In-doped ($Cu_2Sn_{1-x}In_xSe_3$, $x = 0.075$) CTSe at around 700 K [37]. The PF of the samples can be further improved through tuning the chemical composition, or doping the element of Cu or In [37], etc.

Two disk samples were used to characterize the thermal conductivity (κ) along the parallel and perpendicular to the press direction. The thermal transport properties as a function of

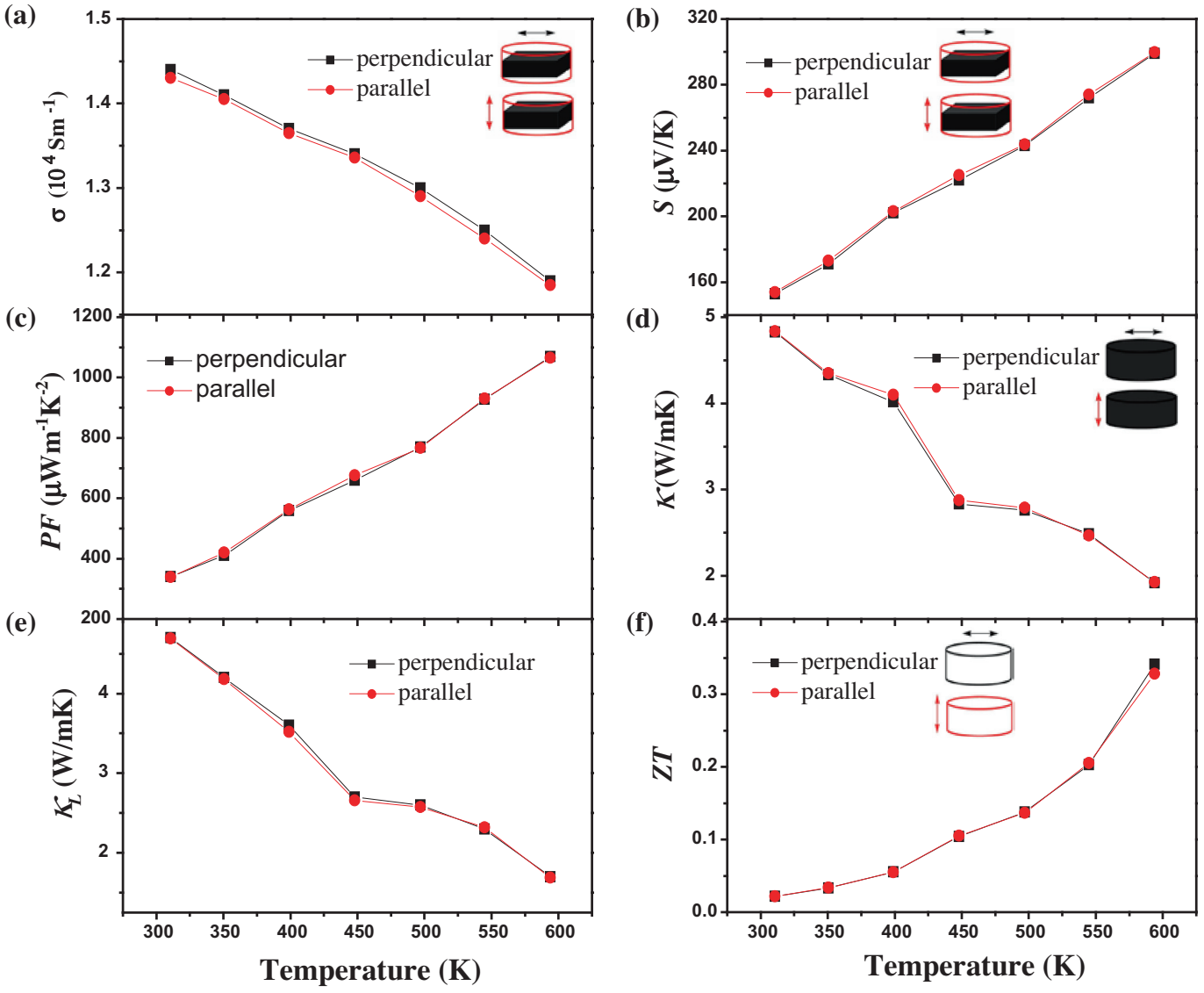

Fig. 5. Temperature dependence of (a) electric conductivity (σ), (b) Seebeck coefficient (S), and (c) power factor (PF), (d) thermal conductivity (κ), (e) lattice thermal conductivities (κ_L), and (f) ZT parallel and perpendicular to the hot-pressing direction. Arrows indicate the directions of the property being measured; the direction of the hot pressing is parallel to the red arrows. (For interpretation of the references to color in this figure legend, the reader is referred to the web version of this article.)

Table 1
The TE properties of CTSe nanocrystals measured at 598 K: the values of σ, S, PF, κ and ZT in both directions, respectively.

Measure direction	σ (Sm^{-1})	S ($\mu V/K$)	PF ($m\,W\,m^{-1}\,K^{-2}$)	κ ($W\,m^{-1}\,K^{-1}$)	ZT
Perpendicular	1.190	299.0	1.07	1.910	0.34
Parallel	1.185	299.8	1.06	1.918	0.33

temperature for CTSe, including thermal diffusivity (Fig. S1) and heat capacity (Fig. S2), are shown in the Supplementary information. As illuminated in Fig. 5d, our compacted materials show thermal conductivities that range from 4.829 $Wm^{-1}\,K^{-1}$ to 1.910 $Wm^{-1}\,K^{-1}$ (perpendicular) and 4.836 $Wm^{-1}\,K^{-1}$ to 1.918 $Wm^{-1}\,K^{-1}$ (parallel) in the ranges of 300 K to 598 K. It is worth noting that the perpendicular thermal conductivity values overlapped on parallel one indicates that thermal conductivity is independence on the measurement directions and kinds of isotropic properties after 450 K. The total thermal conductivity decreases rapidly along with temperature, which indicates that the lattice thermal conductivity makes the major contribution to κ, since σ decreases with temperature. Note that the re-growth of nanocrystals in the dense material is clear (Fig. 4a) during the hot-pressing process. To reduce the re-growth of nanocrystals, better hot-pressing conditions might lead to an even lower thermal conductivity because of size effect. The thermal conductivities of our samples (both at room temperature and at 598 K in two directions) are much larger than κ values reported previously for the undoped CTSe [27] within the measured temperatures ranges and much close to that of the In or Ge-doped CTSe at the corresponding temperature [37,38]. To exclude the contribution of charge carriers in the total thermal conductivity, the Wiedemann–Franz law with a Lorenz number (L_o) of $2.0 \times 10^{-8}\,W\,\Omega\,K^{-2}$ is used [39]. After calculation, it find that the minimum lattice thermal conductivity κ_L ($\kappa = \kappa_L + \kappa_e$) is around 1.70 $W\,m^{-1}\,K^{-1}$ (perpendicular) and 1.68 $W\,m^{-1}\,K^{-1}$ (parallel) of CTSe at 598 K, respectively (Fig. 5e). The reason for the moderate lattice thermal conductivity, which needs to be confirmed by further research, may be the structure distortion caused by different cations or the small grains size of the sample.

According to the above measured data, we calculated the temperature dependence of ZT values by using the electric conductivities, Seebeck coefficients and the thermal conductivities measured perpendicular and parallel to the press direction, which is shown in Fig. 5f. It can be seen that the ZT values of the samples increase with temperature, and the ZT values are isotropic below 550 K, while the dense sample shows a little bit higher ZT value along the perpendicular direction at 598 K. The maximum ZT value of ~0.34 (Table 1) was obtained at 598 K for the CTSe sample along the perpendicular direction, which is a little larger than that the best value (0.3 at 730 K) of undoped bulk CTSe [27], and larger than the figure of merit (0.25 at about 598 K) reported for undoped CTSe [37]. The ZT value might be notably improved with the introduction of controlled amounts of dopants, such as Cu, or Ge [38]. Compared with the previously reported, CTSe or CTSe-based materials, the synthesis temperature of our procedure (180 °C) is much lower, and the reaction time is shortened (30 min); thus, the synthetic method developed here will compete well in energy saving.

4. Conclusions

In summary, we report a "hot-injection" colloidal synthesis strategy for successful synthesis of high production yields ternary CTSe nanocrystals. In this synthesis process, we avoid using the hazardous, unstable alkylphosphines as the organic precursor solution. From TEM analysis, CTSe nanocrystals were monodispersed and quasi-spherical nanoparticles possessed small size with an average diameter of 5 nm. We expect that this lowcost and greener method can be extended to synthesizing high-quality multicomponent nanocrystals such as I–III–VI_2 (I = Cu, Ag; III = Al, In, Ga; VI = S, Se). Finally, we characterized the TE properties of dense materials compacted from those nanocrystals at the temperature of 623 K. The electrical and thermal transport properties have been measured along the perpendicular and parallel to the hot press direction. The as-prepared CTSe nanocrystals exhibited promising TE properties, and the peak ZT value reaches ~0.34 along the perpendicular direction at 598 K, making it possible to capitalize on low-cost solution-based fabrication techniques for use in efficient TE materials applications. Compared to previous reports, we believe that further enhancement of the TE properties can be obtained through proper doping, fine tuning the chemical composition and better controlling the grain size during the compacting procedure.

Acknowledgements

This work is supported by the National Science Foundation of China (NSFC) (Grants 21071002, 21173001, and 21275006), Natural Science Foundation of Anhui Province, China (Grant No. 11040606M34), the Key Project of Anhui Provincial Education Department (KJ2010A014), Financed by the 211 Project of Anhui University, and The Key Laboratory of Environment Friendly Polymer Materials of Anhui Province.

Appendix A. Supplementary material

Supplementary data associated with this article can be found, in the online version, at http://dx.doi.org/10.1016/j.jallcom.2013.07.119.

References

[1] G. Chen, M.S. Dresselhaus, G. Dresselhaus, J.P. Fleurial, T. Caillat, Int. Mater. Rev. 48 (2003) 45–66.
[2] L.E. Bell, Science 321 (2008) 1457–1461.
[3] C.J. Vineis, A. Shakouri, A. Majumdar, M.G. Kanatzidis, Adv. Mater. 22 (2010) 3970–3980.
[4] S.-H. Yang, T.-J. Zhu, T. Sun, J. He, S.-N. Zhang, X.-B. Zhao, Nanotechnology 19 (2008) 245707. 5pp.
[5] J.P. Heremans, V. Jovovic, E.S. Toberer, A. Saramat, K. Kurosaki, A. Charoenphakdee, S. Yamanaka, G.J. Snyder, Science 321 (2008) 554–557.
[6] Y. Liu, L.-D. Zhao, Y.-C. Liu, J.-L. Lan, W. Xu, F. Li, B.-P. Zhang, D. Berardan, N. Dragoe, Y.-H. Lin, C.-W. Nan, J.-F. Li, H.-M. Zhu, J. Am. Chem. Soc. 133 (2011) 20112–20115.
[7] J. Li, J.-H. Sui, Y.-L. Pei, C. Barreteau, D. Berardan, N. Dragoe, W. Cai, J.-Q. He, L.-D. Zhao, Energy Environ. Sci. 5 (2012) 8543–8547.
[8] G.S. Babu, Y.B.K. Kumar, Y.B.K. Reddy, V.S. Raja, Mater. Chem. Phys. 96 (2006) 442–446.
[9] G.H. Chandra, O.L. Kumar, R.P. Rao, S. Uthanna, Mater. Sci. 46 (2011) 6952–6959.
[10] D.-H. Kuo, W.-D. Haung, Y.-S. Huang, J.-D. Wu, Y.-J. Lin, Thin Solid Films 518 (2010) 7218–7221.
[11] L.T. Berger, V.D. Prochukhan, Ternary Diamond-Like Semiconductors, Consultants Bureau, New York, 1969.
[12] G. Marcano, L.M. de Chalbaud, C. Rincón, G.S. Pérez, Mater. Lett. 53 (2002) 151–154.
[13] J.-L. Yao, J.T. Nathan, L.S. Megan, S.P. David, Peter E.R. Blanchard, H.-Y. Gou, A. Mar, C.L. Exstrom, S.A. Darveau, Pierre F.P. Poudeu, Jennifer A. Aitken, Phys. Rev. B 84 (2011) 075203.
[14] J.-H. Li, Q. Tan, J.-F. Li, J. Alloys. Comp. 551 (2013) 143–149.
[15] D.-X. Liang, R.-S. Ma, S.-H. Jiao, G.-S. Pang, S.-H. Feng, Nanoscale 4 (2012) 6265–6268.
[16] T. Plirdpring, K. Kurosaki, A. Kosuga, T. Day, S. Firdosy, V. Ravi, G.J. Snyder, A. Harnwunggmoung, T. Sugahara, Y. Ohishi, H. Muta, S. Yamanaka, Adv. Mater. 24 (2012) 3622–3626.
[17] E.J. Skoug, J.D. Cain, D.T. Morelli, Appl. Phys. Lett. 98 (2011) 261911.

[18] C. Sevik, T. Çağın, Appl. Phys. Lett. 95 (2009) 112105.
[19] F.-J. Fan, B. Yu, Y.-L. Zhu, X.-J. Liu, S.-H. Yu, Z.-F. Ren, J. Am. Chem. Soc. 133 (2011) 15910–15913.
[20] M.-L. Liu, I.-W. Chen, F.-Q. Huang, L.-D. Chen, Adv. Mater. 21 (2009) 3808–3812.
[21] M. Ibáñez, D. Cadavid, R. Zamani, N. García-Castelló, V. Izquierdo-Roca, W.-H. Li, A. Fairbrother, J.D. Prades, A. Shavel, J. Arbiol, A. Pérez-Rodríguez, J.R. Morante, A. Cabot, Chem. Mater. 24 (2012) 562–570.
[22] R. Chesta, W. Aree, P. Wutthisak, Y. Anucha, C. Anek, S. Tosawat, J. Alloys Comp. 509 (2011) 4588–4594.
[23] X.-Y. Shi, F.-Q. Huang, M.-L. Liu, L.-D. Chen, Appl. Phys. Lett. 94 (2009) 122103.
[24] G. Marcano, C. Rincón, L.M. De Chalbaud, D.B. Bracho, G.S. Pérez, J. Appl. Phys. 90 (2001) 1847–1853.
[25] G.E. Delgado, A.J. Mora, G. Marcano, C. Rincón, Mater. Res. Bull. 38 (2003) 1949–1955.
[26] J. Jeong, H. Chung, Y.C. Ju, J. Moon, J. Roh, S. Yoon, Y.R. Do, W. Kim, Mater. Lett. 64 (2010) 2043–2045.
[27] M. Ibáñez, D. Cadavid, U. Anselmi-Tamburini, R. Zamani, S. Gorsse, W.-H. Li, A.M. López, J.R. Morante, J. Arbiol, A. Cabot, J. Mater. Chem. A 1 (2013) 1421–1426.
[28] Michelle E. Norako, Matthew J. Greaney, Richard L. Brutchey, J. Am. Chem. Soc. 134 (2012) 23–26.
[29] L.-Q. Chen, H.-Q. Zhan, C.-L. Liang, M.-M. Wu, J.-Y. Fang, CrystEngCommun 12 (2010) 4386–4391.
[30] X.-G. Peng, J. Wickham, A.P. Alivisatos, J. Am. Chem. Soc. 120 (1998) 5343–5344.
[31] Y. Liu, D. Yao, L. Shen, H. Zhang, X.-D. Zhang, B. Yang, J. Am. Chem. Soc. 134 (2012) 7207–7210.
[32] S.-J. Li, Z.-C. Zhao, Q.-H. Liu, L.-J. Huang, G. Wang, D.-C. Pan, H.-J. Zhang, X.-Q. He, Inorg. Chem. 50 (2011) 11958–11964.
[33] NIST-XPS database, version 3.5. <http://srdata.nist.gov/xps/> (accessed Nov 30, 2011).
[34] L.D. Partain, R.A. Schneider, L.F. Donaghey, P.S. Mcleod, J. Appl. Phys. 57 (1985) 5056–5065.
[35] J.F. Moulder, W.F. Stickle, P.E. Sobol, K.D. Bomben, Handbook of X-ray Photoelectron Spectroscopy, Perkin-Elmer, Eden Prairie, MN, 1992.
[36] M.-Y. Chiang, S.-H. Chang, C.-Y. Chen, F.-W. Yuan, H.-Y. Tuan, J. Phys. Chem. C 115 (2011) 1592–1599.
[37] X.-Y. Shi, L.-L. Xi, J. Fan, W.-Q. Zhang, L.-D. Chen, Chem. Mater. 22 (2010) 6029–6031.
[38] E.J. Skoug, J.D. Cain, D.T. Morelli, J. Alloys. Comp. 506 (2010) 18–21.
[39] A. Bejan, A.D. Kraus, Heat Transfer Handbook, J. Wiley & Sons, 2003, pp. 1338–1340.